Title: Pre-strain Effect on Twist Springback of a 3D P-Channel in Deep Drawing

Authors: Shanshan Chen, Juan Liao, Hongliang Xiang, Xin Xue, António B. Pereira

PII: S0924-0136(19)30180-3
DOI: https://doi.org/10.1016/j.jmatprotec.2019.05.005
Reference: PROTEC 16224

To appear in: *Journal of Materials Processing Technology*

Received date: 15 January 2019
Revised date: 16 April 2019
Accepted date: 10 May 2019

Please cite this article as: Chen S, Liao J, Xiang H, Xue X, Pereira AB, Pre-strain Effect on Twist Springback of a 3D P-Channel in Deep Drawing, *Journal of Materials Processing Tech.* (2019), https://doi.org/10.1016/j.jmatprotec.2019.05.005

Article

Pre-strain Effect on Twist Springback of a 3D P-Channel in Deep Drawing

Shanshan Chen[1], Juan Liao[1,*], Hongliang Xiang[1], Xin Xue[1], António B. Pereira[2]

[1] School of Mechanical Engineering and Automation, Fuzhou University, Fuzhou 350116, Fujian, China, n170220079@fzu.edu.cn (S.C.), xhl@fzu.edu.cn (H.X.), xin@fzu.edu.cn (X.X.)

[2] Department of Mechanical Engineering, University of Aveiro, Aveiro 3810-193, Portugal, abastos@ua.pt

***** Correspondence: jliao@fzu.edu.cn; Tel.: +86-059122866793

Abstract: With the widely use of high-strength steel sheets in the automotive industry, the twist springback phenomenon of the steel sheets under multi-step forming conditions has received extensive attention. In this work, the Dual Phase steel DP500 is taken as the research object to investigate the complex non-linear elastoplastic behaviors and twist springback under two-step loading paths. The large specimen with a pre-strain of 4% true strain in rolling direction is carried out on a large tensile testing machine, and several specific blanks are extracted from it at different directions for a subsequent P-channel forming. The influence of twist springback associated with the pre-strain is analyzed. The finite element model based on the non-linear elastic model and the homogeneous anisotropic hardening model (HAH) is also established for the springback prediction and stress analysis. The results indicate that the pre-strain has a considerable impact on the twist

springback. The non-linear strain path changes resulted from pre-straining not only influence the residual stress but also affect the elastic modulus distribution.

Keywords: Strain path; pre-strain; twist springback; HAH

1. Introduction

Lightweight strategies by using advanced high strength steels (AHSS) are able to contribute to environmentally friendly products with low energy consumption in all fields of industrial application (Lesch, et al., 2017). Dual phase (DP) steel, as one of the widely used AHSS, is attracted for automobile production because of its superior performance including high strength and good plasticity (Schmitt, et al., 2018). However, the springback problems of DP steel caused after sheet metal forming process are serious due to the relatively high level of elastic deformation. Furthermore, the non-linear elastoplastic behavior of the sheet under non-proportional loading is likely to induce more complicate springback (Takamura, et al., 2011). In particular for the hat-shaped channels, springback not only causes a longitudinal offset, but also a certain degree of twist (Pham, et al., 2014). This phenomenon can be defined as twist springback. In the past decades, many researchers have focused on two-dimensional problem of springback, but the attention on three dimensional twist springback is relatively less.

With the plastic strain related loading and unloading, the elastic modulus will decrease (Yang, et al., 2016), and it is found that the elastic modulus is an essential parameter affecting springback (Hassan, et al., 2015). Meanwhile, to better predict the springback of sheet metal forming under non-proportional loading conditions, the strain-hardening model under strain path changes are particularly important and should be considered. Previous studies (Liu et al., 2017; Zajkani et al., 2017) achieved better prediction accuracy in roll forming and U-bending by considering the non-linear elastic modulus. Furthermore, other

works (Xue et al., 2016; Lee et al., 2012) revealed that the use of variable elastic modulus combined with advanced hardening criteria, such as the homogeneous anisotropic hardening (HAH) model, could further improve the simulation results. All the above works demonstrated that the advanced elastoplastic constitutive models can achieve good predictions on 2d tension/compression or U/V bending cases.

Automotive components such as channels are often produced through multi-step forming process due to their complicated geometry. The pre-strain deformation and complex strain path induced in previous process can significantly affect the following material behavior (Xin, et al., 2015) as well as the springback of the parts (Sarker, et al., 2014). In NUMISHEET 2011 conference: The benchmark 4 of pre-strain problems attracted attentions. The research about pre-strain effect on springback of 2d bending test as well as its accurate modeling was proposed (Chung, et al., 2011). Pre-strain may influence the elastoplastic transition in the initial stage of reloading. Yoshida et al. (2002) observed the phenomenon of transient softening and hardening stagnation in reloading. Verma et al. (2011) found that there was apparent permanent softening in the bottom portion of a U-shaped part after a pre-strained tension. Meanwhile, the elastic modulus also got changed during the pre-strain, which influence the springback as well. Both the work of Chongthairungruang et al. (2012) and Yue et al. (2018) revealed that a greater degree of pre-strain could lead to a larger springback. Choi et al., (2017) found that the springback of a U part has been significantly decreased under a double-stage bending, mainly due to the apparent changes in sidewall stress resulted from the strain path changes. Their works indicate that the pre-strain in the former step can result in stress and elastic modulus variation, which obviously influences the springback.

With the rapid development of manufacturing techniques and more complex forming processes, the twist springback of channels in multi-stage loading process has been paid more attention. In this work, the effect of pre-strain on the twist springback of a P-shaped DP

channel is investigated. Aiming at accurately describing the material behavior of the sheet, non-linear elastic model and the advanced distortional hardening model, i.e. HAH model, are used to simulate the pre-strain and forming process. A deep analysis focused on the strain path histories, elastic modulus distribution as well as the sensitivity of the pre-strain directions is further presented.

2. Experiment

2.1. Material

In this paper, dual-phase steel sheet DP500 with a thickness of 0.8 mm is selected. The chemical compositions are shown in the Table 1. The basic mechanical properties identified from the standard tensile tests are summarized in Table 2.

Table 1 Chemical composition of DP500 material (wt%).

C	Si	Mn	P	S	N	Cr	Ni	Al	Cu	V	B
0.079	0.31	0.65	0.009	0.003	0.003	0.03	0.03	0.038	0.01	0.01	0.0003

Table 2 Mechanical properties of DP500 steel sheet.

Initial Elastic modulus E_0 (GPa)	Poisson's ratio ν	Initial yield stress σ_0 (MPa)	Initial yield stress σ_{45} (MPa)	Initial yield stress σ_{90} (MPa)
198	0.3	390	410	398

2.2. Pre-strain and forming experiment

The pre-strain experiment is carried out on a universal tensile testing machine with a capacity of 100kN as shown in Fig. 1a. A novel grip system is designed for the fixture of the large-scale specimen. The size of the large specimen is shown in Fig. 1b, which is optimized by a number of trail-and-error iterations based on experiments and simulations to confirm

that the strain distribution is uniform in the middle region. Recently, Zaman et al. (2017) also conducted a pre-strain experiment with a large-scale specimen, it pointed out that the flow stress and yield trajectory can be better analyzed for subsequent non-coaxial loading only when the pre-strained sheet size is large enough and the strain distribution is sufficiently uniform. In this work, the large specimen is first stretched to a true strain of 4% in the rolling direction (RD). A corresponding extensometer is used for the strain recording of the large specimen. After that, the blank of the forming part is cut from the center region of the pre-strained sheet. Thereafter, the blank is transferred to a forming tool and a P-shaped channel is formed. The whole process is schematically illustrated in Fig. 2. The shape of the P-channel can be described as a varied cross section along a guide line, as shown in Fig. 2a ③. In order to better investigate the pre-strain effect on the following forming process, the blank is cut along (Fig. 2a) or in the transverse direction (Fig. 2b) from the pre-strain axis, respectively. According to the angle between the guide line of the formed part and the pre-strain axis (also the RD of the material), we called P-channel (RD) if the angle is 0°, whereas P-channel (TD) if 90°.

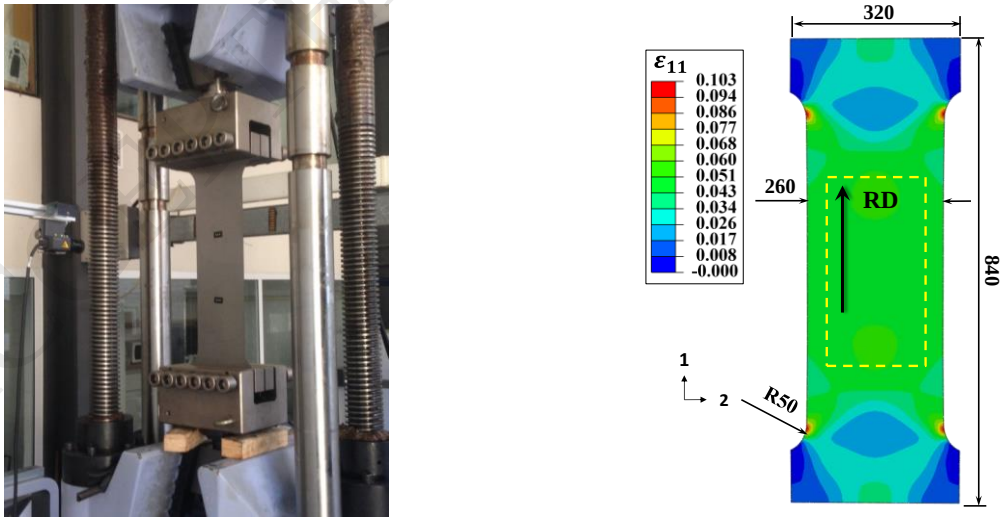

(**a**) (**b**)

Fig. 1 Pre-strain experiment: (**a**) the tensile testing machine equipped with a large grip system (**b**) the size of the large specimen and strain distribution (ε_{11}).

The main functional part of the forming tool includes a punch, a die, a blank holder and a distant plate. Six gas springs are positioned under the blank holder to maintain a maximum blank holding force of 144kN, as illustrated in Fig. 3a. The final formed parts are shown in Fig. 3b. Those who are interested in the experimental device can refer to the literature (Liao, et al., 2017a) for more details.

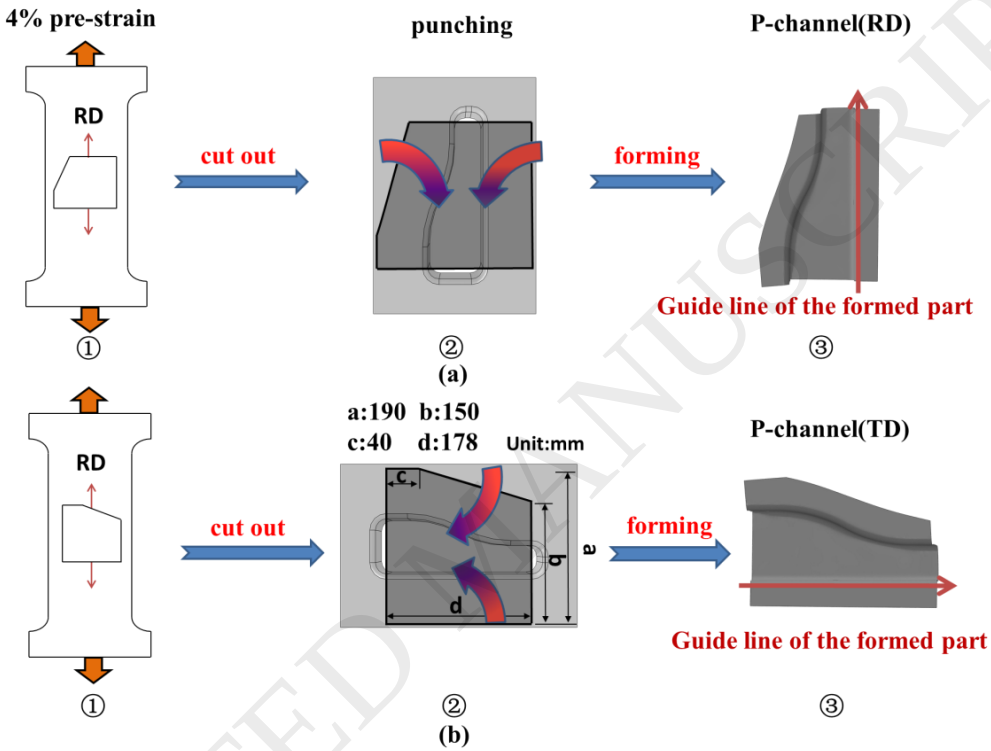

Fig. 2 Schematic illustration of the pre-strain and forming process: forming along (**a**) the pre-strain axis and (**b**) 90° from the pre-strain axis.

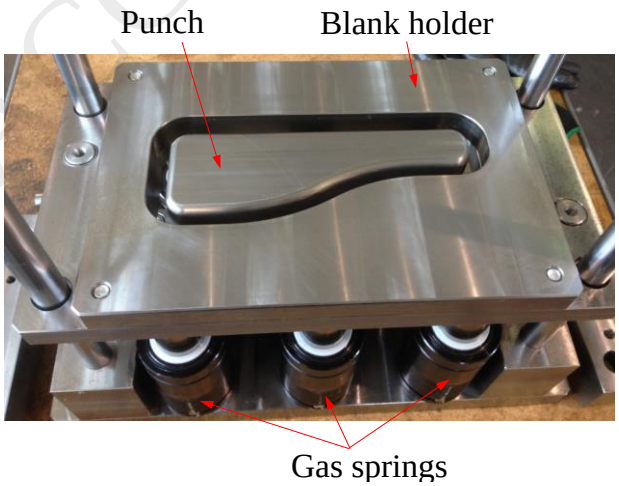

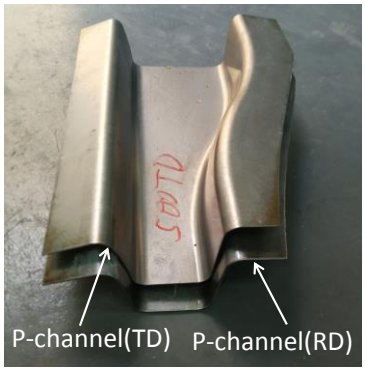

(**a**) (**b**)

Fig. 3 (**a**) The lower half part of forming tool and (**b**) the formed parts.

3. Constitutive modeling and finite element simulation

The forming process of the channel part is non-proportional and it always involves severe strain path changes. In order to characterize the non-linear material behavior under different strain path changes during the multi-loading processes, the anisotropic yield function Yld2000-2d integrated with a distortional hardening model (i.e. HAH model) is adopted in this work. Moreover, a Chord model (Yoshida, et al., 2002) is also used to characterize the elastic modulus, which varies with the increase of the plastic strain. Both of the elastic and hardening models have been proved to affect the twist springback prediction significantly (Liao, et al., 2017a).

3.1. Non-linear elastic model

Yoshida et al. (2002) proposed a Chord modulus model, which indicates that the elastic modulus appears to decrease continuously in the process of increasing the equivalent strain. The mathematical expression is as follows:

$$E_{\text{chord}} = E_0 - (E_0 - E_{\text{a}})[1 - \exp(-\zeta \bar{\varepsilon}_p)] \tag{1}$$

In this formula, E_0 is the initial elastic modulus, E_{a} is expressed as Chord modulus based on plastic strain, ζ corresponds to material parameter, and $\bar{\varepsilon}_p$ represents equivalent plastic strain. The three coefficients in this model for the DP500 are identified from the uniaxial loading-unloading-loading (ULUL) cycle test (Xue et al., 2016), and the fitted values are listed later in Figure 8(a).

3.2. The distortional hardening (HAH) model

The adopted distortional hardening model is called HAH (homogeneous yield function-based anisotropic hardening) model. The incipient HAH model (Barlat, et al.,

2011) is put forward to represent the Bauschinger effect at load reversal. Thereafter, Barlat et al. (2013, 2014) further improved it to describe conditions under non-proportional loadings. The enhanced HAH model can capture the stress evolutions under the cross-loading. Its yield criterion is:

$$\bar{\sigma}(\mathbf{s}) = (\phi^{q} + \phi_{h}^{q})^{\frac{1}{q}} = ([\sqrt{\phi(\mathbf{s}')^{2} + \phi(\mathbf{s}'')^{2}}]^{q} + f_{1}^{q}\left|\hat{\mathbf{h}}:\mathbf{s} - \left|\hat{\mathbf{h}}:\mathbf{s}\right|\right|^{q} + f_{2}^{q}\left|\hat{\mathbf{h}}:\mathbf{s} + \left|\hat{\mathbf{h}}:\mathbf{s}\right|\right|^{q})^{\frac{1}{q}} = \sigma(\bar{\varepsilon}) \tag{2}$$

Where q is the constant exponent, it controls distortion of the yield surface when load reverses, $\mathbf{s}$ is the stress deviation, f_1 and f_2 represent the state variable. The stable component ϕ and the fluctuation component ϕ_h constitute the yield surface $\bar{\sigma}(\mathbf{s})$. The fluctuation component ϕ_h can get the yield surface distorted according to degree of the applied load. The yield surface of the stable component ϕ is the reference before distortion. The $\hat{\mathbf{h}}$ is a tensor which is known as the microstructure deviator. The reference stress-strain curve $\sigma(\bar{\varepsilon})$ is to signify the isotropic hardening of material. The initial value of $\hat{\mathbf{h}}$ corresponds to the stress deviation associated with the first incremental step of plastic deformation. Evolution of state variables depends on the sign of $\hat{\mathbf{h}}:\mathbf{s}$, which illustrates more in Appendix A.

$$\cos\chi = \frac{\hat{\mathbf{h}}:\mathbf{s}}{\sqrt{\hat{\mathbf{h}}:\hat{\mathbf{h}}}\sqrt{\mathbf{s}:\mathbf{s}}} = \mathrm{H}\hat{\mathbf{h}}:\hat{\mathbf{s}} \tag{3}$$

The cosχ in the formula (3) is an important indicator of the strain path. It represents the angular relationship between $\hat{\mathbf{h}}$ and $\mathbf{s}$. The value cosχ=1 accounts for the monotonic loading, cosχ=-1 for the reverse loading and cosχ=0 for the cross-loading condition.

3.3. Model verification

In the HAH model, a dislocation density-based hardening model (Rauch, et al., 2007) is adopted as the referenced isotropic hardening model, this model can capture the work hardening stagnation during the load reversal. The equation of the classical expression is:

$$\sigma(\bar{\varepsilon}) = M[\tau_0 + \alpha\mu b\sqrt{\rho(\bar{\varepsilon})}] \tag{4}$$

The parameter M represents the average Taylor factor, τ_0 is the friction stress, α is a coefficient signifying dislocation interactions, μ is elastic shear modulus, b characterizes the length of the Burgers vector and the $\rho(\bar{\varepsilon})$ is a state variable associated with stress. The more details about state variable evolutions are introduced in Appendix B. Parameter values in this model and the Yld2000-2d yield function are listed in Table 3. The parameters of the HAH model are also shown in Table 3, in which the q is set to 2 as suggested by literature (Barlat, et al., 2014). The fitting parameters of the HAH model are eight. Among them, the parameters $k_{1\text{-}5}$ control state changes under load reversal, k, k_s and s are related to cross-loading. More details about the parameter identification are addressed in previous work (Liao, et al., 2017a).

The performance of the HAH model for the non-proportional loading paths can be verified from the Fig. 4, which compared the predicted and experimental stress-strain responses of DP500 in a two-step tensile test (Liao, et al., 2017b). In this test, a large-scale tensile specimen is stretched in the RD direction and then sub-sized tensile samples are cut at different angles from the RD for a second standard tensile test. This test could characterize the materials behavior of the DP steel at a strain path change of cross or near reverse loading. Fig. 4 indicates that a lower reloading yield stress and permanent softening is observed when the loading path changes after 4% pre-strain along the RD. This phenomenon is more severe at the reloading angle of $90°$ (near reverse loading) than that of $45°$ (near cross-loading). Liao et al., (2017b) explored the mechanism of this transient hardening behavior of the dual phase steels and ascribed it to the deformation incompatibilities between the soft ferrite and the hard martensite phase of the dual phase steels.

Fig. 4 also shows that the HAH model captures very well all the material behavior of DP500 under different loading path changes. This can be explained from the Fig. 5, which depicts the yield loci evolution of the distortional hardening model at the π-plane. After a

first loading of 4% pre-strain along the s1-axis, the yield surface flattens at the opposite side, accounting for the Bauschinger effect if the load reverses. Meanwhile, the surface contracts with the maximum effect at any orthogonal direction from the current loading direction. Thus, the transient hardening behavior of the material can be captured when the loading path changes to cross loading.

Table 3 Parameters of the constitutive models for DP500.

Dislocation density-based model	α	M (GPa)	b (nm)	τ_0 (MPa)	M	K	D (μm)	F	P
	0.5	80	0.246	121	3.05	148	20	3.5	0.8
Yld2000-2d	α	α_1	α_2	α_3	α_4	α_5	α_6	α_7	α_8
	6	0.903	1.058	1.029	0.978	0.963	0.743	0.945	1.057
HAH	q	k	k_1	k_2	k_3	k_4	k_5	k_s	s
	2	14	90	33.4	0.48	0.92	5	179	0.833

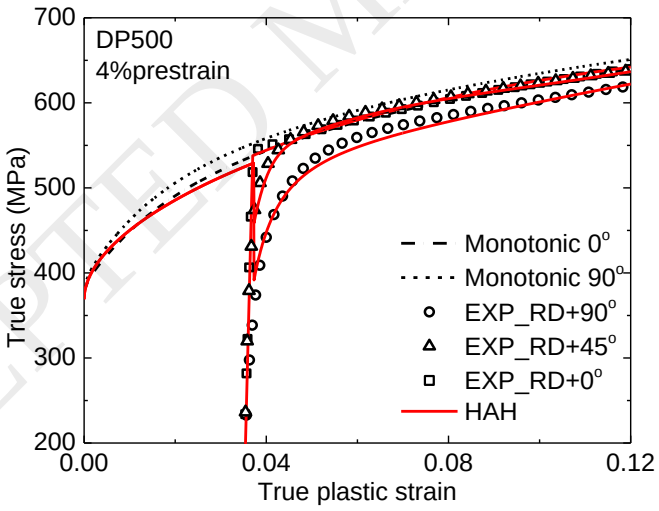

Fig. 4 The stress-strain curves of the DP steel sheet after 4% pre-strain along the rolling direction (RD) followed by a second loading at 0°, 45°, 90° from the pre-strain axis (experimental results and HAH predictions) in a two-step tensile test.

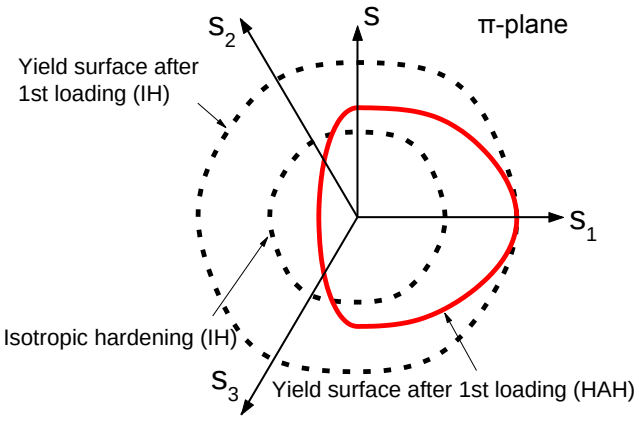

Fig. 5 Yield loci evolutions after isotropic (IH) and distortional hardening (HAH) after 4% pre-strain along the rolling direction.

3.4. Finite element simulation

The HAH model has been implemented in the software ABAQUS through the VUMAT/UMAT subroutines for the numerical simulation. The pre-strain and forming process simulation of the P-channel are divided into four steps: (1) Pre-strain; (2) Springback; (3) Forming; (4) Springback. It has been examined from the pre-strain experiments that the trimming process has very limited effect on the residual strain of the P-blank and can be negligible, thus the simulation of the trimming process is not performed for computational efficiency. The pre-strain simulation is conducted directly on the small blank for the P-channel. The size of the pre-strained blank is the same as the small specimen (as shown in Fig.2①②) cut from the center region of the large specimen. Firstly, the blank sheet is pre-strained to a 4% true strain in the rolling direction. And then the sheet is unloaded for springback. Second, the forming process is performed on the pre-strained blanks along (Fig. 2a) or in the transverse direction (Fig. 2b) of the pre-strain axis, respectively. Finally, the formed part is unloaded again for springback. The implicit time integration scheme with the user subroutine UMAT is used for the pre-strain and springback simulations while the explicit time integration scheme with the VUMAT

subroutine is adopted for the forming simulation. The stress and internal state variables of the elements and their nodes are imported from the last stage while the scheme changes from implicit to explicit or vice versa. The blank is meshed with four-node shell elements (S4R) with the grid size of 1mm×1mm. The thickness integration point is set to 9.

4. Results and discussion

4.1. Evaluation of twist springback

In terms of springback, most studies have been carried out on the 2d springback of equal cross section channels. Respecting the channels with varied cross sections, it is often accompanied by twist deformation. Generally, the twist can be simply evaluated by the relative angle of the bottom line of the cross sections. However, in many cases the bottom surface is also distorted and cannot be used as the reference. Therefore, in order to better characterize the twist deformation of the P-channel, this article evaluates it by the relative twist angle of the different sections by means of the principal axis of inertia, as shown in Fig. 6a. Seven representative cross sections are taken for the measurement of the twist springback for this P-channel.

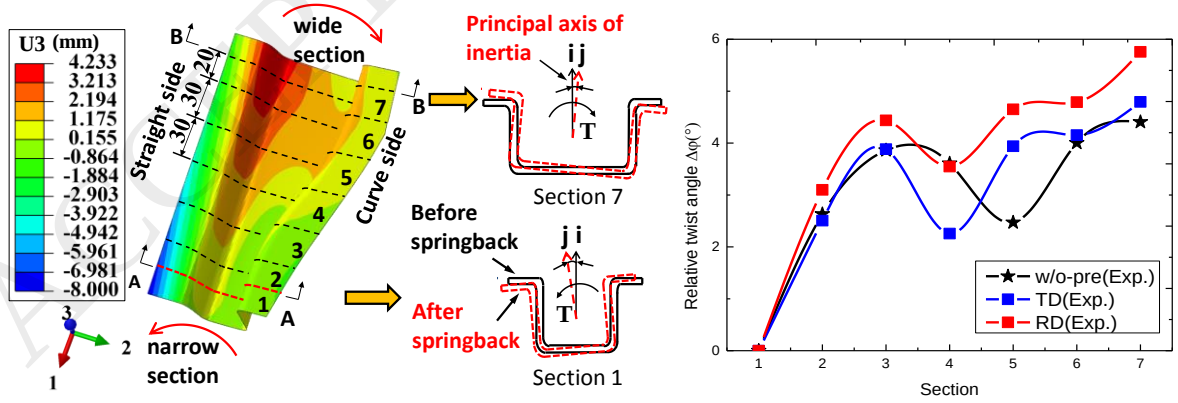

(**a**) (**b**)

Fig. 6 (**a**) Displacement U3 distribution and schematic diagram of twist springback for cross sections and (**b**) comparison of relative twist angles with and without pre-strain.

The vectors **i**, **j** respectively represent the principal axis of inertia before and after the springback, and the absolute twist angle φ of each section is expressed as:

$$\varphi = \cos^{-1} \frac{(\mathbf{i} \cdot \mathbf{j})}{|\mathbf{i}||\mathbf{j}|} \tag{5}$$

The distribution of the displacement at z-axis (U3) is shown as Fig. 6a. It indicates that the entire part has an obvious twist along the longitudinal direction. For a better analysis of the relative twist angle of each section, the narrow section φ_1 is chosen as the reference. Thus the relative twist angle $\Delta\varphi$ is:

$$\Delta\varphi = \varphi_i - \varphi_1 \quad (i=2,3\ldots7) \tag{6}$$

Fig. 6b compared the measured relative twist angle of the pre-strained forming parts with the part without pre-strain. For the part without pre-strain, the twist angle always increases with the length except a short decrease at the transition section 4 and 5. The trend is similar for the pre-strained parts. A little divergence is that the decrease of the twist is more serious at section 4. On the other hand, the twist of the P-channel (RD) is globally larger than that of TD and the maximum relative twist angle approaches to $6°$ at section 7. This will be explained in next section based on the analysis of the stress distribution.

Considering that the pre-strain might has a crucial effect on the springback and this phenomenon may not be fully expressed by the twist angle, the 2d springback of the sections should also be taken into account. The section 1 and 7 is taken as representatives to show the main characteristic of the 2d springback, as shown in Fig. 7. The calculated springback angle and sidewall curl are summarized in Table 4 and 5, in which the subscript ‘s’ or ‘c’ stands for the value at the straight or curved sidewall, respectively.

Obviously, it can be seen that the springback amount of the two pre-strained P-channel (TD/ RD) is much greater than the one without pre-strain, which can be reflected by a much smaller ρ, a larger θ_2 or smaller θ_1. It indicates that the pre-strain brings more springback for

this channel, no matter it forms along RD or TD direction from the pre-strain axis. But the RD channel generates a litter more springback and twist than that of the TD one.

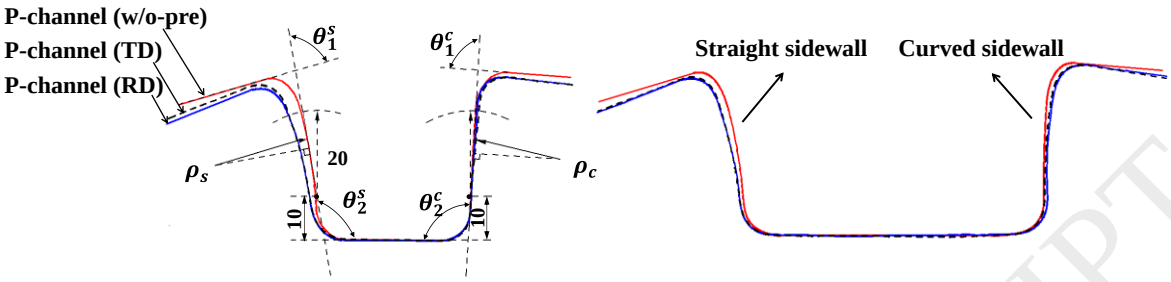

(**a**) section 1 (**b**) section 7

Fig. 7 Springback evaluation method and cross section comparison.

Table 4 Comparison of 2d springback of section 1.

Method	θ_1^s	θ_1^c	θ_2^s	θ_2^c	ρ_s	ρ_c
P-channel (w/o-pre)	83.5	89.0	99.7	93.3	125.0	1000.0
P-channel (TD)	82.9	88.7	104.4	95.9	102.0	531.9
P-channel (RD)	86.5	87.7	104.7	93.9	78.1	561.8

Table 5 Comparison of 2d springback of section 7.

Method	θ_1^s	θ_1^c	θ_2^s	θ_2^c	ρ_s	ρ_c
P-channel (w/o-pre)	83.2	87.1	100.1	91.9	113.6	312.5
P-channel (TD)	81.6	84.5	102.6	93.7	122.0	147.1
P-channel (RD)	81.6	84.9	104.0	93.0	101.0	94.3

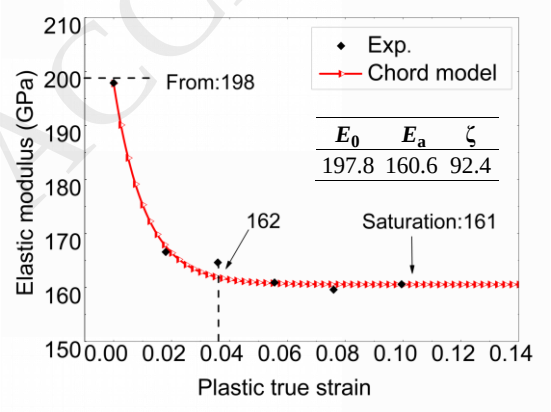

(**a**)

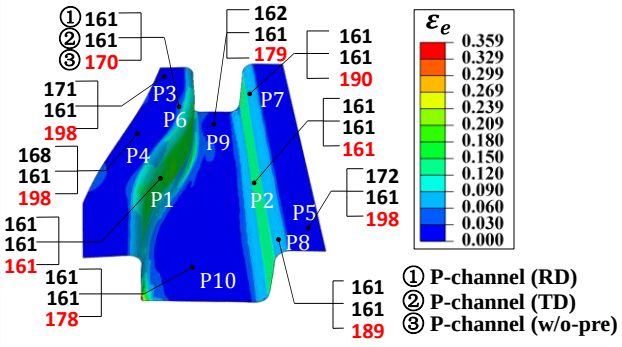

(**b**)

Fig. 8 Effect of plastic strain on elastic modulus: (**a**) The elastic modulus decreases tendency based on the Chord model. (**b**) Equivalent plastic strain distribution (ε_e) and elastic modulus distribution under different loading modes.

In order to explain the larger springback caused by pre-strain, the tendency of the varied elastic modulus with the plastic strain based on ULUL test and the Chord elastic model is shown in Fig. 8a. When the sheet is pre-strained to 4%, there is a significant decrease of the elastic modulus from the initial 198GPa to 162GPa and it almost closes to the saturation of 161GPa. During the forming stage, the elastic modulus also varied according to the equivalent strain. Fig. 8b shows the equivalent strain distribution of the forming part without pre-strain. It also compared the elastic modulus of several representative points for the two pre-strained channels and the one without pre-strain. The elastic modulus at the sidewall are very similar for the three channels, as indicated by P1 and P2, because the plastic strain is large in these areas owing to the restraining of the blank holder force. However, the elastic modulus at the flange (P3, P4, P5), the corner (P6, P7, P8) and the bottom surface (P9, P10) of the channel without pre-strain is much larger than the other two channels, since the latters were already subjected to a pre-strain deformation and the elastic modulus has reached a smaller value. Smaller elastic modulus generates larger springback. This is the main reason why the pre-strain results in larger springback of the two P-channels (RD/TD). Comparing the two pre-strained channels, the elastic modulus distribution of the P-channel (RD) is a little more inhomogeneous than that of TD, which might be related with the strain path history.

4.2. Stress and strain path analysis

Twist springback is generally caused by the torsional moment formed by residual stress and the uneven stress distribution of the entire component. For the P-channel, the strain path probably changes in the non-proportional multi-loading process and this will cause the

difference of stress distribution. In order to better analyze the influence of strain path changes on the stress distribution, the simulated residual stress of the channels after the forming process are compared.

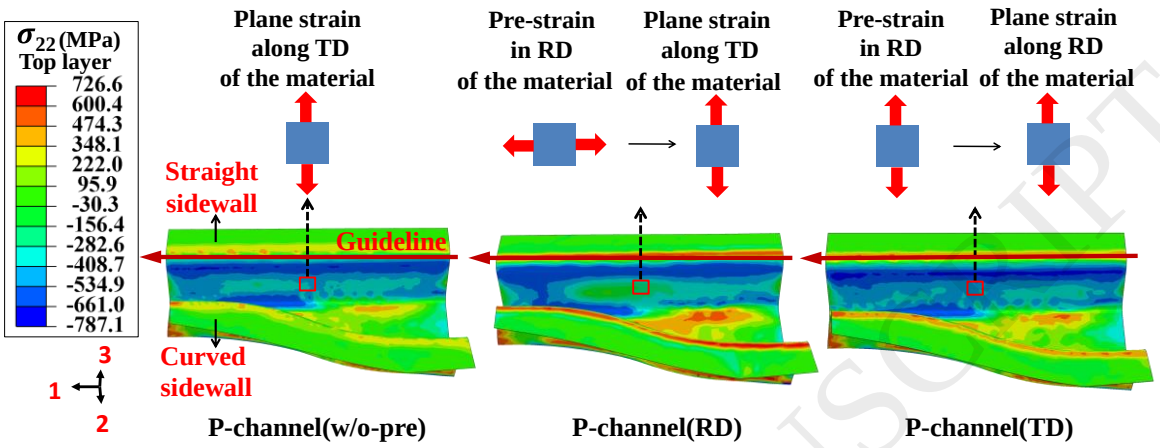

Fig. 9 Stress distribution (σ_{22}) of P-channels and schematic deformation of an element on straight sidewall during pre-strain and forming process.

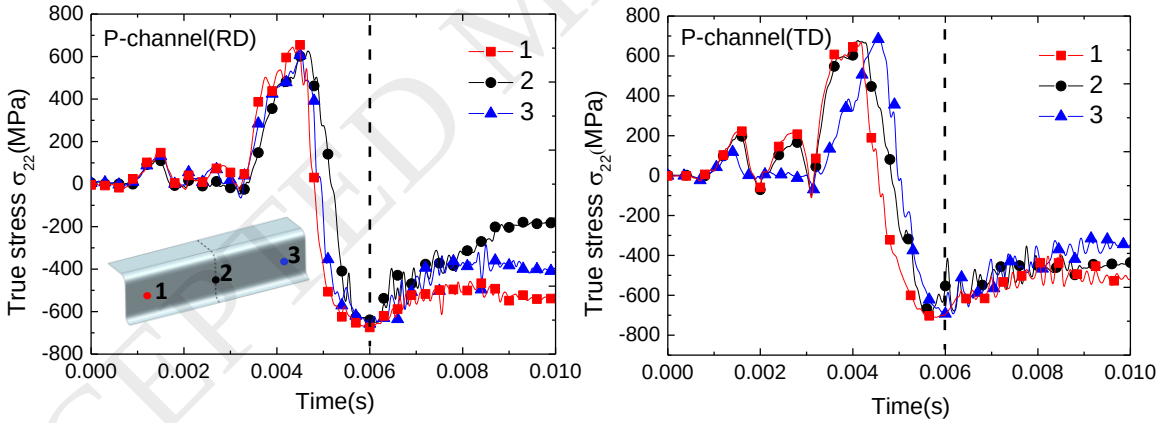

Fig. 10 Stress σ_{22} in different areas of the straight sidewall.

The stress distribution of the straight side is analyzed first. For the straight sidewall, the deformation mode is close to plane strain (Marciniak, et al., 2002). Meanwhile the σ_{11} (the stress along the 1 axis) is very small and can be negligible. Fig. 9 compared the σ_{22} of the three channels, which indicates that stress distribution of the P-channel (RD) is very inhomogeneous, and the stress is smaller than the others in most area of the sidewall. The

heterogeneity of the stress can also be quantitatively reflected from Fig. 10, in which the stress evolution of three points (1, 2, 3) in the sidewall of the P-channel (RD) and (TD) are traced and compared. The divergence of the final stress for the P-channel (RD) is more serious than the one (TD). The maximum gap between point 1 and 2 reaches 350 MPa.

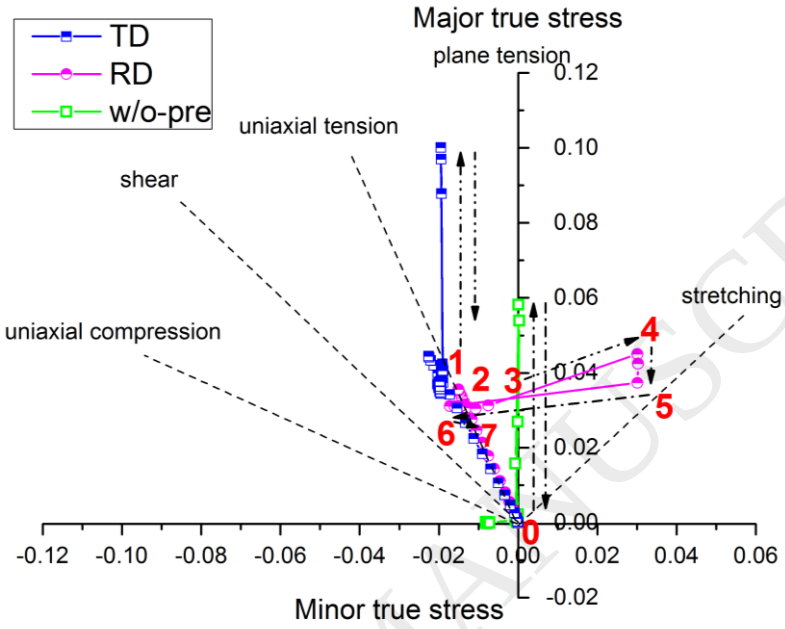

Fig. 11 Strain path changes of point 2 in the pre-strain and forming process.

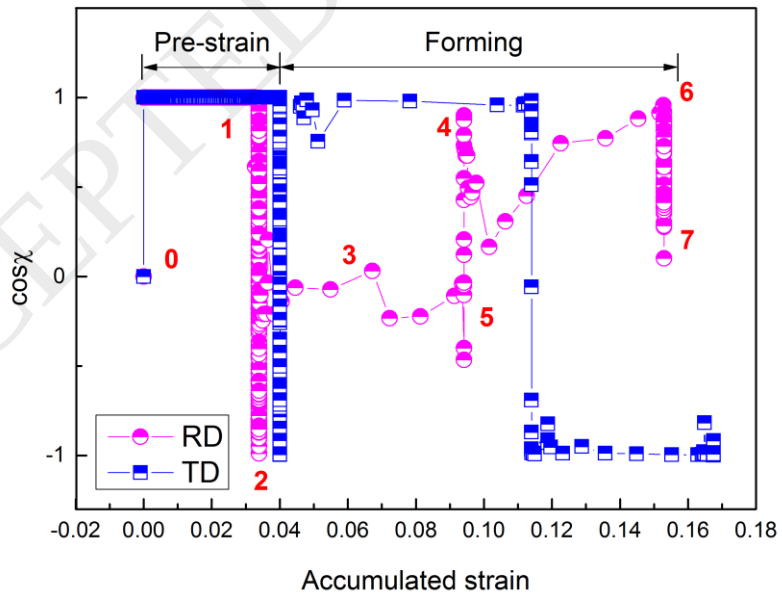

Fig. 12 Evolution of cosχ about point 2.

The stress divergence is mainly ascribed to the different strain paths in the multi-loading process for the three channels. The element 2 (E2) at the straight sidewall of the three channels is taken as an example to show the deformation mode during the two-step loading process, as shown in Fig. 9 and 11. Meanwhile, the cosχ of the E2, which represent the strain path changes in the HAH model, are also traced in Fig. 12 for the pre-strained channels. In the pre-strain step, the sheets are continuously subjected to a uniaxial tension along the rolling direction, as shown in Fig. 11. This corresponds to a monotonic strain path for both of the P-channel RD and TD, which can be reflected from the value cosχ=1 in Fig. 12. During the springback process, the pre-strain stress is released and sometimes several elements might suffer a slight reverse loading when the whole part is reaching a balanced state. Therefore, there is a sudden drop of cosχ to -1 and recover back again for both channels, as indicated in Fig. 12. In the forming step, initially the strain path of the E2 of the channel-RD changes from the uniaxial tension to a plane strain along the transvers direction in the flange, while the E2 of channel-TD changes to a plane strain along the rolling direction, as demonstrated in Fig. 9 and 11. The former is a cross-loading (cosχ≈0), while the latter is between the monotonic and cross-loading situation (cosχ falls to about 0.5 in Fig. 12). Thereafter the material flows from the die radius to the sidewall, the E2 (channel-TD) is subjected to a reverse loading in Fig. 12, which is reflected as a decrease of the cosχ to -1. However, for the E2 (channel-RD), the strain path is more complex due to the effect of the pre-strain and the change of the forming direction. After a near reverse loading (cosχ falls to -0.5), it finally suffers a cross-loading (cosχ changes to 0).

The non-linear strain path histories result in a different stress result for the channels. The stress evolutions of the E2 for the three channels in the forming stage are compared in Fig. 13. There are two considerable divergences for the three channels. The first one is in the start of the forming stage, it could be seen from the enlarged drawing A of Fig. 13, the stress of the channel with pre-strain are larger than that without since they are strain hardened. The

stress of the channel (RD) is lower than that of TD, because it is just subjected to a cross loading (uniaxial tension along RD changes to a plane strain along TD) and the re-yielding stress is lower, which can be retrospected from the Fig. 4. The second gap is in the end of the forming. The final stress of the channel (RD), channel (TD) and channel (w/o-pre) is -182MPa, -436MPa, -493MPa, respectively. The residual stress of the channel (RD) is much lower than the others, which again is due to the cross loading situation at that time. For the channel (TD), it is recovering the monotonic stress after a long time of reverse loading and the stress level is close to the one without pre-strain.

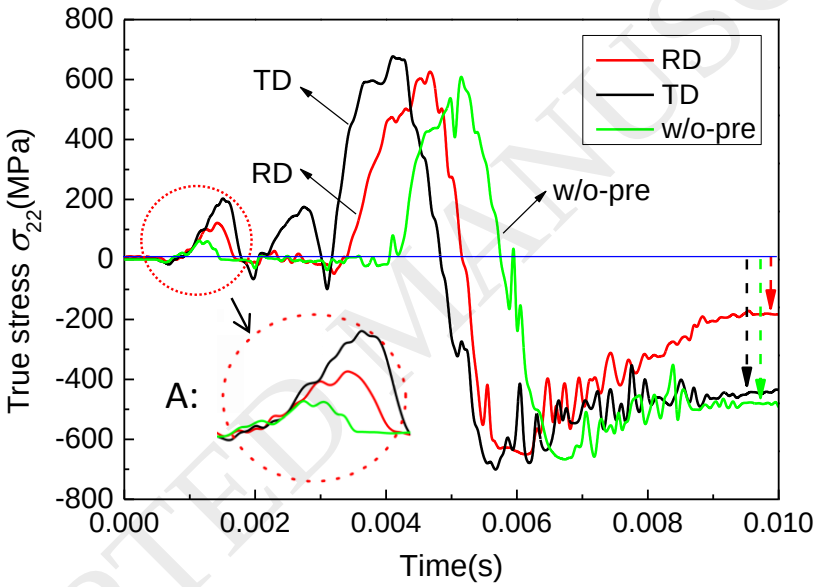

Fig. 13 Evolution of stress σ_{22} under the forming process.

For the curved sidewall, the magnitude and distribution of the stress σ_{11} are closely related to the twist deformation, as explained previously in the literature (Liao, et al., 2017a). The σ_{11} distribution of the two pre-strained channels is illustrated in Fig. 14. It shows that a total opposite stress σ_{11} is distributed in the flange and sidewall due to the curvature of the channel. Tensile stress is concentrated in the sidewall of the wide side while compression stress is concentrated in that of the narrow side. The historic stress evolution of the two areas is also traced in Fig. 14c, which also presents that the stress path

of the two areas is always opposite. During the springback process, the release of the opposite stresses in these areas would result in a twist deformation in accordance with the geometric compatibility (Xue, et al., 2015). Obviously, there is a larger tensile and compression stress level of the channel RD than that of TD, as compared in Fig. 14c. Thus, a larger twist deformation is expected for the channel RD. Furthermore, for both the straight side and curved side, the residual stress and elastic modulus of the channel RD is more inhomogeneous than that of TD due to the complicated strain path history. The uneven stress distribution and heterogeneous elastic modulus are also the triggers of the twist. These are the main reasons why the twist of the channel RD is globally larger than the TD in Fig. 6b.

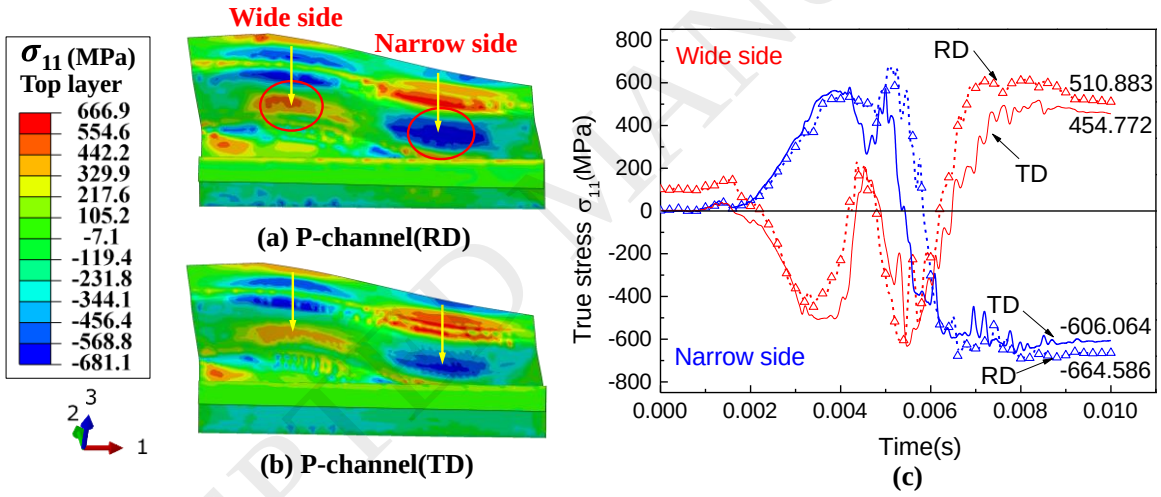

Fig. 14 Stress σ_{11} distribution of (**a**) P-channels (RD) and (**b**) P-channel (TD), (**c**) stress historic evolution of σ_{11} under forming process.

4.3. Comparison between different elastic models

In section 4.2, it shows that the change of elastic modulus after pre-strain has a considerable effect on the twist springback, and the pre-strained P-channels generate larger springback than that without pre-strain deformation.

In order to better analyze the effect of elastic modulus model on the twist springback prediction, Fig. 15 compares the different results predicted by HAH model integrated with the constant elastic modulus E_0 and the Chord elastic model. The average deviation denoted as 'Dev' is used to express the error between the predicted results of different elastic models and the experiment. It is calculated according to the following formula:

$$\mathrm{Dev} = \frac{\frac{1}{\mathrm{N}}\sum_{i=1}^{\mathrm{N}}\left|\Delta\hat{\varphi}_i - \Delta\varphi_i'\right|}{\sum_{i=1}^{\mathrm{N}}\left|\overline{\Delta\hat{\varphi}_i}\right|} \times 100\% \tag{7}$$

$$\Delta\varphi_i = \left|\Delta\hat{\varphi}_i - \Delta\varphi_i'\right| \quad (i=2,3\ldots7) \tag{8}$$

$\Delta\hat{\varphi}_i$ and $\Delta\varphi_i'$ represent the relative twist angles of the experiment and simulation, respectively. The value N represents the number of sections. The $\Delta\varphi_i$ characterizes the deviation of the relative twist angle of section *i*.

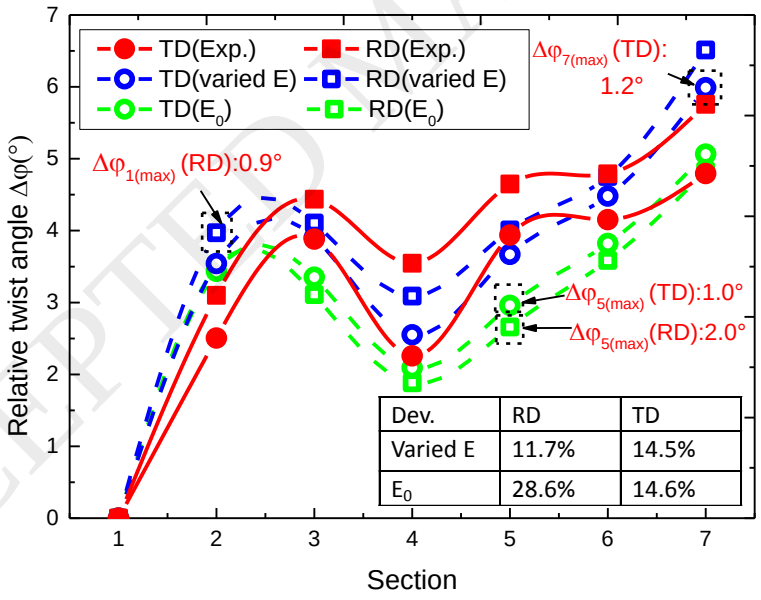

Fig. 15 Comparison of relative twist angles based on different elastic models.

It can be seen from Fig. 15 that the tendency of all the predicted results agrees well with the experiment. Obviously for both channel RD and TD, the simulated results by E_0 globally underestimated the twist springback, which is due to an overestimation of the elastic modulus

after the pre-strain. The average deviation (Dev.) of P-channel (RD) and P-channel (TD) by Chord model are 11.7% and 14.5%, which are smaller than that predicted by E_0. The latter are 28.6% and 14.6%, respectively.

Fig. 15 also indicates that the average deviation of channel (RD) predicted by E_0 is the largest among all the models. The maximum deviation of the relative twist angle is $2°$, also occurring at section 5 of the channel (RD) by model with E_0. This might ascribe to the heterogeneous elastic modulus distribution of the channel (RD) after the non-linear strain paths. The more complicated strain path changes in the multi-step loading process of channel (RD) causes inhomogeneous plastic strain, which results in heterogeneous elastic modulus distribution, as demonstrated in Fig. 8b. The model with constant E_0 ignores the variation of the elastic modulus during the complex strain path, resulting in the largest deviation of twist springback prediction.

5. Conclusion

In order to study the effect of pre-strain on twist springback of a P-channel, a large-scale DP steel sheet is pre-strained first and then cut at different directions for a subsequent P-shaped channel forming experiment. The strain path evolution and elastic modulus variation in the process are analyzed based on the finite element simulations, which take into account an advanced distortional hardening model (HAH) and the Chord elastic model. Some conclusions are drawn as follows:

(1) The twist springback predictions by the HAH model integrated with the Chord elastic model are in good agreement with the experiment. The strain path evolutions are also studied by tracing the values of the $\cos\chi$ in the HAH model. The result indicates that the two-step forming process induces non-linear strain path changes, which significantly affect the residual stress distribution.

(2) A sensitivity study of the pre-strain axis demonstrates that the pre-strain axis is directly related to the stress distribution. When the pre-strain axis is in line with the guide line of the channels, the straight side wall would experience cross-loading which results in a decrease of residual stress for the partial channel. This is the main reason of the uneven stress distribution of formed parts and the trigger of the more severe twist deformation.

(3) A degradation of elastic modulus after the pre-strain causes obvious 2d springback (angular change of sections), regardless of the pre-strain direction. Meanwhile, the non-linear strain path history also has a significant impact on the elastic modulus. The inhomogeneous plastic strain brings about heterogeneous elastic modulus distribution, which is also one of the relevant causes of the twist springback.

Acknowledgments: The authors wish to express their special appreciation to Prof. Frédéric Barlat of Pohang University of Science and Technology and Prof. Myoung Gyu Lee of Seoul National University for sharing the user-material subroutine code of the HAH model. This work was supported by the NSFC (National Natural Science Foundation of China) under the project (51805087), the Natural Science Foundation of Fujian province of China (2018J01761), the Major Science and Technology Project in Fujian Province (2017HZ0001-2) and the Open test funding project for valuable instruments in Fuzhou University (2019T014).

Appendix A

When the material experiences strain path changes, the state variables in the HAH model evolves as follows. For reverse loading,

If $\hat{\mathbf{h}}:\hat{\mathbf{s}}\geq 0$:

$$\frac{\mathrm{d}g_1}{\mathrm{d}\bar{\varepsilon}} = k_2(k_3\frac{\bar{\sigma}_0}{\sigma(\bar{\varepsilon})} - g_1) \tag{A1}$$

$$\frac{\mathrm{d}g_2}{\mathrm{d}\bar{\varepsilon}} = k_1\frac{g_3 - g_2}{g_2} \tag{A2}$$

$$\frac{\mathrm{d}g_4}{\mathrm{d}\bar{\varepsilon}} = k_5(k_4 - g_4) \tag{A3}$$

$$\frac{\mathrm{d}\hat{\mathbf{h}}}{\mathrm{d}\bar{\varepsilon}} = k\mathrm{b}\left[\left|\frac{\cos\chi}{\mathrm{H}}\right|^{1/z} + g_R\right](\hat{\mathbf{s}} - \cos\chi\hat{\mathbf{h}}) \tag{A4}$$

If $\hat{\mathbf{h}}:\hat{\mathbf{s}}<0$:

$$\frac{\mathrm{d}g_1}{\mathrm{d}\bar{\varepsilon}} = k_1\frac{g_4 - g_1}{g_1} \tag{A5}$$

$$\frac{\mathrm{d}g_2}{\mathrm{d}\bar{\varepsilon}} = k_2(k_3\frac{\bar{\sigma}_0}{\sigma(\bar{\varepsilon})} - g_2) \tag{A6}$$

$$\frac{\mathrm{d}g_3}{\mathrm{d}\bar{\varepsilon}} = k_5(k_4 - g_3) \tag{A7}$$

$$\frac{\mathrm{d}\hat{\mathbf{h}}}{\mathrm{d}\bar{\varepsilon}} = k\mathrm{b}\left[\left|\frac{\cos\chi}{\mathrm{H}}\right|^{1/z} + g_R\right](-\hat{\mathbf{s}} + \cos\chi\hat{\mathbf{h}}) \tag{A8}$$

In Eq. (A4) and Eq. (A8),

$$\mathrm{b} = \mathrm{sgn}(\cos\chi),\ \mathrm{sgn\,x} = \begin{cases} 1\ , \mathrm{x} \geq 0 \\ -1\ , \mathrm{x} < 0 \end{cases} \tag{A9}$$

$$\frac{\mathrm{d}g_R}{\mathrm{d}\bar{\varepsilon}} = k_R[k_R^{'}(1-\cos^2\chi) - g_R] \tag{A10}$$

For $\cos\chi=0$ (i.e. cross-loading), there are two options which can be activated separately or simultaneously

$$\frac{\mathrm{d}g_L}{\mathrm{d}\bar{\varepsilon}} = k_L[\frac{\sigma(\bar{\varepsilon}) - \bar{\sigma}_0}{\sigma(\bar{\varepsilon})}(\sqrt{L(1-\cos^2\chi) + \cos^2\chi} - 1) + 1 - g_L] \tag{A11}$$

$$\frac{\mathrm{d}g_s}{\mathrm{d}\bar{\varepsilon}} = k_s[1+(S-1)\cos^2\chi - g_s] \tag{A12}$$

k, $k_{1\text{-}5}$, S, k_s, L and k_L, these constants are all material coefficients, g_1 and g_2 are applied to characterize the Bauschinger effect, g_3 and g_4 represent permanent softening, g_s is related to transient hardening and g_L is the parameter to capture the amplitude of the transient yield surface extension during the cross-loading.

Appendix B

This dislocation density-based hardening model put forward by Rauch et al. (2007) is to capture the work hardening stagnation at load reversal. The $\rho(\bar{\varepsilon})$ is a state variable associated with stress which is composed of forward ρ_f and reverse ρ_{r}.

$$\rho(\bar{\varepsilon}) = \rho_f + \rho_{\mathrm{r}} \tag{A13}$$

The model is embedded in enhanced HAH model, evolution of state variables is closely related to the sign of $\hat{\mathbf{h}}:\hat{\mathbf{s}}$.

If $\hat{\mathbf{h}}:\hat{\mathbf{s}} \geq 0$:

$$\frac{\mathrm{d}\rho_{f1}}{\mathrm{d}\gamma} = \frac{\sqrt{\rho_{f1}}}{bK} + \frac{1}{bD} - k\rho_{f1} \tag{A14}$$

$$\frac{\mathrm{d}\rho_{\mathrm{r}1}}{\mathrm{d}\gamma} = -(\frac{\sqrt{\rho_{f1}}}{bK} + \frac{1}{bD})\frac{\rho_{\mathrm{r}1}}{\rho_{f01}} \tag{A15}$$

$$\rho_{f2} = (1-p)\rho_{f1} + \rho_{\mathrm{r}1}, \rho_{\mathrm{r}2} = p\rho_{f1}, \rho_{f02} = \rho_{f1}, \rho(\bar{\varepsilon}) = \rho_{f1} + \rho_{\mathrm{r}1} \tag{A16}$$

If $\hat{\mathbf{h}}:\hat{\mathbf{s}} < 0$:

$$\frac{\mathrm{d}\rho_{f2}}{\mathrm{d}\gamma} = \frac{\sqrt{\rho_{f2}}}{bK} + \frac{1}{bD} - k\rho_{f2} \tag{A17}$$

$$\frac{\mathrm{d}\rho_{\mathrm{r}2}}{\mathrm{d}\gamma} = -(\frac{\sqrt{\rho_{f2}}}{bK} + \frac{1}{bD})\frac{\rho_{\mathrm{r}2}}{\rho_{f02}} \tag{A18}$$

$$\rho_{f1} = (1-p)\rho_{f2} + \rho_{r2}, \rho_{r1} = p\rho_{f2}, \rho_{f01} = \rho_{f2}, \rho(\bar{\varepsilon}) = \rho_{f2} + \rho_{r2} \tag{A19}$$

In Eq. (A14-15) and Eq. (A17-18),

$$\mathrm{d}\gamma = M\mathrm{d}\bar{\varepsilon} \tag{A20}$$

K, *D*, *k* and *p* fully characterize material coefficients, among them, *K* and *D* represent a number of forest dislocations cut and the grain size, respectively. ρ_{f1}, ρ_{r1} and ρ_{f2}, ρ_{r2} correspond to two situations respectively where the value of $\hat{\mathbf{h}}:\hat{\mathbf{s}}$ is greater or less than zero. ρ_{f01} and ρ_{f02} are the dislocation density when $\hat{\mathbf{h}}:\hat{\mathbf{s}}$ sign changes.

References

Barlat, F., Gracio, J.J., Lee, M.G., Rauch, E.F., Vincze, G., 2011. An alternative to kinematic hardening in classical plasticity. Int. J. Plast. 27, 1309-1327.

Barlat, F., Ha, J., Gracio, J.J., Lee, M.G., Rauch, E.F., Vincze, G., 2013. Extension of homogeneous anisotropic hardening model to cross-loading with latent effects. Int. J. Plast. 46, 130-142.

Barlat, F., Vincze, G., Gracio, J.J., Lee, M.G., Rauch, E.M., Tome, C.N., 2014. Enhancements of homogenous anisotropic hardening model and application to mild and dual-phase steels. Int. J. Plast. 58, 201-218.

Choi, J., Lee, J., Bong, H.J., Lee, M.G., Barlat, F., 2017. Advanced constitutive modeling of advanced high strength steel sheets for springback prediction after double stage U-draw bending. Int. J. Solids Struct. 151, 152-164.

Chongthairungruang, B., Uthaisangsuk, V., Suranuntchai, S., Jirathearanat, S., 2012. Experimental and numerical investigation of springback effect for advanced high strength dual phase steel. Mater. Des. 39, 318-328.

Chung, K., Kuwabara, T., Verma, R.K., Park T., Huh, H., Bae, G., 2011. BM4: Pre-strain effect of spring-back of 2-D draw bending, The NUMISHEET 2011 Benchmark Study of the 8th International Conference and Workshop on Numerical Simulation of 3D Metal Forming Processes, Seoul, Korea, pp. 171-208.

Hassan, H.U., Maqbool, F., Guner, A., Hartmaier, A., Khalifa, N.B., Tekkaya, A.E., 2015. Springback prediction and reduction in deep drawing under influence of unloading modulus degradation. Int. J. Mater. Form. 9, 619-633.

Lee, J.Y., Lee, J.W., Lee, M.G., Barlat, F., 2012. An application of homogeneous anisotropic hardening to springback prediction in pre-strained u-draw/bending. Int. J. Solids Struct. 49, 3562-3572.

Lesch, C., Kwiaton, N., Klose, F.B., 2017. Advanced High Strength Steels (AHSS) for Automotive Applications − Tailored Properties by Smart Microstructural Adjustments. Steel Research International. 88, 1700210.

Liao, J., Xue, X., Lee, M.G., Barlat, F., Vincze, G., Pereira, A.B., 2017a. Constitutive modeling for path-dependent behavior and its influence on twist springback. Int. J. Plast. 93, 64-88.

Liao, J., Sousa, J.A., Lopes, A.B., Xue, X., Barlat, F., Pereira, A.B., 2017b. Mechanical, microstructural behaviour and modelling of dual phase steels under complex deformation paths. Int. J. Plast. 93, 269-290.

Liu, X.L., Cao, J.G., Chai, X.T., Liu, J., Zhao R.G., Kong, N., 2017. Investigation of forming parameters on springback for ultra high strength steel considering Young's modulus variation in cold roll forming. J. Manuf. Process. 29, 289-297.

Marciniak, Z., Duncan, J.L., Hu, S.J., 2002. Mechanics of Sheet Metal Forming, 2rd ed. 90 Tottenham Court Road, London, England, pp. 33-35.

Pham, C.H., Thuilier, S., Manach, P.Y., 2014. Twisting analysis of ultra-thin metallic sheets. J. Mater. Process. Technol. 214, 844-855.

Rauch, E.F., Gracio, J.J., Barlat, F., 2007. Work-hardening model for polycrystalline metals under strain reversal at large strains. Acta. Mater. 33, 2939-2948.

Sarker, D., Chen, D. L., 2014. Dependence of compressive deformation on pre-strain and loading direction in an extruded magnesium alloy: Texture, twinning and de-twinning. Mate. Sci. Eng. A 596, 134-144.

Schmitt, J.H., Iung, T., 2018. New developments of advanced high-strength steels for automotive applications. C. R. Phys. 19, 641-656.

Takamura, M., Fukui, A., Yano, H., Hama, T., Sunaga, H., Makinouchi, A., Asakawa, M., 2011. Investigation on Twisting and Side Wall Opening Occurring in Curved Hat Channel Products Made of High Strength Steel Sheets. Proc. NUMISHEET 2011, 887

Verma, R.K., Chung, K., Kuwabara, T., 2011. Effect of pre-strain on anisotropic hardening and springback behavior of an ultra low carbon automotive Steel. ISIJ Int. 51, 482-490.

Xin, Y.C., Zhou, X.J., Wu, Y., Yu, H.H., Liu, Q., 2015. Deformation behavior and mechanical properties of composite twin structures under different loading paths. Mate. Sci. Eng. A 640, 118-128.

Xue, X., Liao, J., Vincze, G., Barlat, F., 2015. Twist springback characteristics of dual-phase steel sheet after non-axisymmetric deep drawing. Int. J. Mater. Form. 10, 267-278.

Xue, X., Liao, J., Vincze, G., Pereira, A.B., Barlat, F., 2016. Experimental assessment of nonlinear elastic behaviour of dual-phase steels and application to springback prediction. Int. J. Mech. Sci. 117, 1–15.

Yang, X., Choi, C., Sever, N.K., Altan, T., 2016. Prediction of springback in air-bending of Advanced High Strength steel (DP780) considering Young's modulus variation and with a piecewise hardening function. Int. J. Mech. Sci. 105, 266-272.

Yoshida, F., Uemori, T., Fujiwara, K., 2002. Elastic–plastic behavior of steel sheets under in-plane cyclic tension–compression at large strain. Int. J. Plast. 18, 633-659.

Yue, Z.M., Qi, J.S., Zhao, X.D., Badreddine, H., Gao, J., Chu, X.R., 2018. Springback Prediction of Aluminum Alloy Sheet under Changing Loading Paths with Consideration of the Influence of Kinematic Hardening and Ductile Damage. Metals, 8, 950.

Zajkani, A., Hajbarati, H., 2017. Investigation of the variable elastic unloading modulus coupled with nonlinear kinematic hardening in springback measuring of advanced high-strength steel in U-shaped process. J. Manuf. Process. 25, 391-401.

Zaman, S.B., Barlat, F., Kim, J.H., 2017. Deformation-induced anisotropy of uniaxially prestrained steel sheets. Int. J. Solids Struct. 134, 20-29.